PROCEEDINGS B

royalsocietypublishing.org/journal/rspb

Research

Cite this article: Smith SM, Angielczyk KD. 2020 Deciphering an extreme morphology: bone microarchitecture of the hero shrew backbone (Soricidae: *Scutisorex*). *Proc. R. Soc. B* **287**: 20200457.
http://dx.doi.org/10.1098/rspb.2020.0457

Received: 27 February 2020
Accepted: 31 March 2020

Subject Category:
Morphology and biomechanics

Subject Areas:
biomechanics, evolution

Keywords:
trabecular bone, vertebrae, micro-computed tomography, shrews, functional morphology, extreme morphology

Author for correspondence:
Stephanie M. Smith
e-mail: smsmith@fieldmuseum.org

Electronic supplementary material is available online at https://doi.org/10.6084/m9.figshare.c.4938126.

THE ROYAL SOCIETY PUBLISHING

Deciphering an extreme morphology: bone microarchitecture of the hero shrew backbone (Soricidae: *Scutisorex*)

Stephanie M. Smith and Kenneth D. Angielczyk

Field Museum of Natural History, Negaunee Integrative Research Center, 1400 South Lake Shore Drive, Chicago, IL 60605-2496, USA

SMS, 0000-0002-7480-3581

Biological structures with extreme morphologies are puzzling because they often lack obvious functions and stymie comparisons to homologous or analogous features with more typical shapes. An example of such an extreme morphotype is the uniquely modified vertebral column of the hero shrew *Scutisorex*, which features numerous accessory intervertebral articulations and massively expanded transverse processes. The function of these vertebral structures is unknown, and it is difficult to meaningfully compare them to vertebrae from animals with known behavioural patterns and spinal adaptations. Here, we use trabecular bone architecture of vertebral centra and quantitative external vertebral morphology to elucidate the forces that may act on the spine of *Scutisorex* and that of another large shrew with unmodified vertebrae (*Crocidura goliath*). X-ray micro-computed tomography (µCT) scans of thoracolumbar columns show that *Scutisorex thori* is structurally intermediate between *C. goliath* and *S. somereni* internally and externally, and both *Scutisorex* species exhibit trabecular bone characteristics indicative of higher *in vivo* axial compressive loads than *C. goliath*. Under compressive load, *Scutisorex* vertebral morphology is adapted to largely restrict bending to the sagittal plane (flexion). Although these findings do not solve the mystery of how *Scutisorex* uses its byzantine spine *in vivo*, our work suggests potentially fruitful new avenues of investigation for learning more about the function of this perplexing structure.

1. Introduction

The relationship between morphology and function is a central concept in the study of structural evolution. Connecting an organism's morphology to its biomechanical capabilities is critical to understanding how it interacts with its environment, as well as how organisms adapt to selective pressures and ecological opportunities. Structures with unique or extreme morphologies are problematic in this context because they often lack an obvious function and are not readily comparable to homologues or analogues in other organisms. The problem is especially severe for cryptic or extinct organisms where opportunities for the direct observation of function are limited or non-existent.

The hero shrew has a spinal column unlike that of any other known vertebrate. Most of its dorsal vertebrae, including at least half of the thoracic vertebrae and all lumbar vertebrae, have dorsoventrally expanded lateral processes whose cranial and caudal faces are covered in fingerlike bumps or tubercles (figure 1, [1–4]). These tubercles articulate with those of neighbouring vertebrae, such that the dorsal spine forms a dense column of tightly interlocking bony processes (figure 1). *Scutisorex* also has more lumbar vertebrae than other shrews; most soricids have five lumbar vertebrae, whereas *Scutisorex thori* has eight and *S. somereni* has 10–12 [1,2].

The function of this highly modified spine is enigmatic. *Scutisorex* has been the subject of intense anatomical inspection and description [1–7], but functional investigations have been inconclusive. Early reports [4] suggested that the robust spine

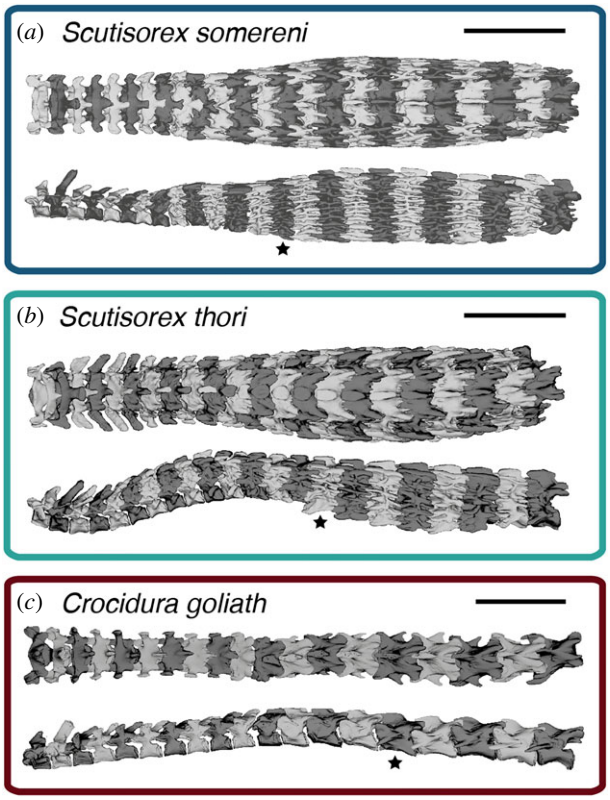

Figure 1. Dorsal (above) and lateral (below) view of thoracic and lumbar vertebrae for each species in this study. Cranial is to the left. Colours alternated to show interdigitation of tubercles and zygapophyses. Scale bars are all 10 mm. Specimens are FMNH 137613 (*S. somereni*), FMNH 219669 (*S. thori*), and FMNH 162144 (*C. goliath*). Black stars indicate the first lumbar vertebra. (Online version in colour.)

of *S. somereni* allowed it to bear the weight of an adult human and escape unscathed, but no field or laboratory observations have been made of any behaviours that clearly necessitate its radical morphology. Cullinane & Bertram [8] showed that the intervertebral joints of *S. somereni* are highly resistant to axial torsion. They also found that the lumbar spine of *S. somereni* does not behave as a series of viscoelastic joints under compression, but instead as a single rigid bar. Despite observing a captive specimen alive for several months, Cullinane & Aleper [1] were unable to pinpoint an *in vivo* use for the vertebral column that benefits from this property. Histological work shows that the unusually modified transverse processes of the vertebrae develop endochondrally, precluding interpretations of the morphology as pathological [6].

The discovery of a second species, *S. thori* [2], provided a critical new data point for understanding the evolution of the *Scutisorex* spine. Along with having an intermediate number of lumbar vertebrae, *S. thori* has fewer, larger tubercles on its vertebrae than does *S. somereni* (figure 1). This discovery did not yield any new functional clues, but it was hypothesized that *S. thori* might also represent a functional intermediate between a normal spine and the extreme modification found in *S. somereni*. Stanley *et al*. [2] suggested that the robust spine might be used in flexion to pry palm leaves away from the main trunk of the plant, giving access to nutritious insect larvae, but this behaviour has not been observed. Instead, *S. somereni* has been found to eat mostly earthworms and is, therefore, at least a semi-subterranean forager [9], and it resembles other small fossorial mammals in having robust ribs for its body size. Yet, *S. somereni* does not have unusually stout limbs, and in fact has long bone proportions comparable to those of non-fossorial mammals [7].

Because *Scutisorex* vertebrae are so radically modified, it is difficult to compare them morphometrically to more typical vertebral columns while also capturing the likely functionally relevant parts of the morphology. We attempt to circumvent this problem by inspecting not only the external morphology of the *Scutisorex* spine, but also the internal morphology via centrum trabecular bone architecture (TBA). According to a set of principles commonly referred to as 'Wolff's Law' [10–13], the structure of trabecular bone can provide quantitative information about the physical loads experienced by a bone *in vivo*. The relationship between TBA, *in vivo* loads, and bone function has been studied in a variety of mammals, including primates [14–19], artiodactyls [20–22], rabbits [23,24], squirrels [25,26], bats [27], and murid rodents [28–31]. This work shows that direction, magnitude, and frequency of load are physically manifest in the trabecular structure of the loaded bone, and we use that phenomenon to elucidate trabecular features that might relate to the function of the *Scutisorex* spine.

Although soricid trabecular bone has been studied in the context of allometric scaling of bone characteristics among mammals [32], no studies of trabecular bone have been conducted exclusively on shrews. In light of this, we have several specific aims: (i) to quantify the internal and external morphology of *Scutisorex* dorsal vertebrae, and their range of inter- and intraspecific variation, (ii) for comparison, to quantify internal and external morphology of the dorsal spine in the closely related, 'unmodified' shrew, *Crocidura goliath*, which is similar in size to both *Scutisorex* species, (iii) to determine the degree to which *S. thori* represents an intermediate between *S. somereni* and *C. goliath*, in both TBA metrics and external morphology, (iv) to assess the relationship between TBA variation and external characteristics of the vertebrae, including number of tubercles in *Scutisorex*, and (v) connect morphology and variation through the column to functional hypotheses and the limited existing behavioural data on *Scutisorex*.

2. Methods

(a) Specimen selection and micro-computed tomography scanning

We executed X-ray micro-computed tomography (µCT) scans of the thoracic and lumbar vertebrae of 20 specimens: 13 specimens of *S. somereni*, 3 specimens of *S. thori* (the total worldwide sample of the taxon currently available in natural history museums), and 4 specimens of *C. goliath* (table 1). All specimens are from the Field Museum of Natural History (FMNH), and all are adult based on epiphyseal fusion of limb bones. We scanned specimens using the 240 kV tube of the GE v|tome|x µCT scanner at the University of Chicago PaleoCT facility. Because of differences in size and spine orientation, isotropic voxel size ranged from 14 to 26 µm. In some cases, thoracic and lumbar vertebrae were scanned separately; when necessary, we scanned both at the same or similar resolutions to minimize intra-specimen variation in scan quality (electronic supplementary material, table S2). We reconstructed specimens in GE phoenix datos|x and aligned and cropped the resulting image stacks using VGStudio MAX 3.3 (Volume Graphics, 2019).

Table 1. Thoracic and lumbar vertebral counts for all specimens in this study. FMNH 223983 (denoted with an asterisk) has one additional transitional lumbar–sacral vertebra, which is fused to the first sacral and was therefore not included due to several measurements being inaccessible. Holotype of *Scutisorex thori* denoted with a double asterisk. 'alc' is a specimen preserved in alcohol.

specimen no.	taxon	prep type	sex	mass (g)	thoracic count	lumbar count	total trunk vertebrae
FMNH 137613	*Scutisorex somereni*	dry	M	67	13	11	24
FMNH 148270	*Scutisorex somereni*	dry	?	59	13	12	25
FMNH 148271	*Scutisorex somereni*	dry	F	69	14	11	25
FMNH 148941	*Scutisorex somereni*	dry	F	65.5	14	11	25
FMNH 160178	*Scutisorex somereni*	dry	M	54.5	13	11	24
FMNH 189277	*Scutisorex somereni*	dry	F	53	14	10	24
FMNH 223983*	*Scutisorex somereni*	alc	M	81	13	10*	23*
FMNH 227556	*Scutisorex somereni*	alc	F	76	13	11	24
FMNH 219669**	*Scutisorex thori*	dry	F	47	14	8	22
FMNH 222612	*Scutisorex thori*	alc	M	36	14	8	22
FMNH 222613	*Scutisorex thori*	alc	M	49	14	8	22
FMNH 162144	*Crocidura goliath*	alc	F	58	14	5	19
FMNH 162185	*Crocidura goliath*	dry	M	51	14	5	19
FMNH 162186	*Crocidura goliath*	dry	F	52	14	5	19
FMNH 167691	*Crocidura goliath*	alc	M	57	15	5	20

(b) Data collection: external morphology

To separate vertebral scans, we imported image stacks into ORS Dragonfly 4.0 (Object Research Systems, 2019) and exported each vertebra individually as an stereolithography (STL) mesh. We cleaned each vertebral model and separated it from any remaining pieces of neighbouring vertebrae using Autodesk Meshmixer 3.5.474. Using the 'Units/Dimensions' function in Meshmixer, we took four linear measurements on each thoracic and lumbar vertebra of all three included species (electronic supplementary material, figure S8). In the two species of *Scutisorex*, we also quantified the number of tubercles projecting from the cranial and caudal surfaces of each vertebra. To standardize and record the number of tubercles present, we opened the STL of the vertebra in Meshmixer in orthographic view, aligned the model with the craniocaudal axis of the vertebral centrum perpendicular to the plane of the screen and took screenshots of the cranial and caudal faces of the specimen. We divided the image of the vertebra into four quadrants, with a horizontal line tangent to the top of the centrum delineating dorsal and ventral sections, and a vertical line at the mediolateral midpoint of the centrum and neural arch (electronic supplementary material, figure S8). We recorded the number of tubercles in each quadrant, with a tubercle defined as a relatively small-diameter peglike or bumplike feature with a local maximum in the cranial or caudal direction on the vertebral surface, not including zygapophyses. We specify 'relatively small-diameter' because we excluded local maxima on the edges of the vertebral centrum (i.e. the cranial and caudal extents of the centrum itself). We also excluded transverse processes where they are clearly identifiable. Three-dimensional models of all *Scutisorex* thoracic and lumbar vertebrae are available for download from Morphosource (www.morpho source.org, Project #P956).

(c) Data collection: trabecular bone architecture

For our analysis of the TBA of each vertebral centrum, we sought to maximize the volume of trabecular bone we used while (i) excluding all cortical bone, (ii) as much as possible, sampling the same relative proportion of the total bone structure in each vertebra and across species, and (iii) analysing regions of interest (ROIs) from the same location in each vertebra. To keep our sampling as standardized as possible, we first aligned the vertebra in Dragonfly so that the dorsal side of the vertebral centrum paralleled the *z*-axis; the dorsoventral axis of the centrum paralleled the *x*-axis; and the mediolateral axis of the vertebra paralleled the *y*-axis. We then selected the largest square prism possible inside the centrum while including only trabecular bone. The resulting ROIs typically measured 0.6–1.2 mm per side (mostly 0.75–0.85 mm), and 1.0–3.25 mm in craniocaudal length.

We exported TIFF stacks of our hexahedral ROIs and executed binary thresholding in Fiji [33]. We acknowledge that the small size of the structures we are attempting to detect makes choice of segmentation method critical to the validity of our results, and we therefore, tested three segmenting methods to determine which would provide the most accurate binary renderings of our broader dataset. These tests are detailed in the electronic supplementary material, Section A, and figures S1–S7. Based on results of these tests, we chose to use Otsu segmenting [34] for our main body of analyses. Although Otsu segmentation could potentially result in slight underestimation of bone volume fraction (BVF) and trabecular thickness (Tb.Th), and slight overestimation of dispersal of trabecular direction away from the craniocaudal axis, it is effective at maintaining thin trabecular structures during segmenting, and less subject to user subjectivity and overestimation of trabecular parameters than global grey value threshold segmenting. Furthermore, relative resolutions (mean Tb.Th divided by scan resolution, resulting in pixels per trabecular structure; [35]) for all specimens in our study are between 1.52 and 5.48 pixels/trabecula, with an average of 3.00 px/tb. This value is not unreasonably low compared to that of other studies (see electronic supplementary material). Therefore, any error is likely to be systematic, and similar in magnitude across specimens, and will probably not affect our interpretation of bone qualities in the species relative to one another. Otsu threshold is determined using the grey value histogram for the entire stack of images to which it is applied; stacks with high and low BVF have inherently different histogram parameters, and will, therefore, be thresholded slightly differently by the Otsu procedure. However, the difference in attenuation between bone and air is

large, providing a clear distinction between bone and background, and we therefore, do not expect the difference in histograms to have a notable effect on our results. We applied Otsu thresholding via the Fiji plugin Auto Threshold, v. 1.16.5 (https://github.com/fiji/Auto_Threshold) [36]. ROI image stacks, both pre- and post-Otsu thresholding, and results of alternate segmenting methods used in supplementary analyses are available on Morphosource (www.morphosource.org, Project #P956); raw data for sensitivity tests are available on the Dryad Digital Repository (https://doi.org/10.5061/dryad.8w9ghx3hf).

We calculated four structural metrics for our trabecular bone ROIs: BVF, trabecular number (Tb.N), Tb.Th, and primary trabecular orientation in the form of trend and plunge relative to the transverse plane of the vertebra. We conducted these analyses on thresholded ROI stacks in Quant3D [37,38] with a user-defined threshold of 127–255; 2049 uniform rotations; dense vectors and random rotations turned on; omit side intersecting paths turned on; and star volume and star length distributions calculated with 2000 points. We also used a centred sphere (figure 2) as the volume of interest for these calculations, to eliminate edge-related artefacts. To visualize primary trabecular orientation, we plotted trend and plunge for each vertebra using Stereonet 10 [39,40]. Raw data for these analyses are available on the Dryad Digital Repository (https://doi.org/10.5061/dryad.8w9ghx3hf).

Because our segmenting protocol is automated, it reduces user-introduced error in segmenting and subsequent error in TBA metrics. Yet, there is still a degree of uncertainty in our reported values, because slight variations in threshold can cause variation in TBA results. To estimate the uncertainty in our results, we used a subset of specimens to determine the mean deviation from our reported values when we increased or decreased the automatic Otsu threshold by 10%. We used these values to construct ranges of uncertainty for BVF, Tb.Th, and Tb.N, with the size of the range customized to reflect the volatility of the metric in response to changing threshold (electronic supplementary material, table S1). Details of this procedure are presented in the electronic supplementary material, Section B; and the image stacks with increased and decreased threshold used to determine uncertainty are available on Morphosource (Project #P956). Uncertainty ranges are applied to the species mean line for each species across all three metrics in figure 5, and are reported numerically in a separate tab of the supplementary data on the Dryad Digital Repository.

It is important to note that although our ROIs are smaller than those examined in larger animals such as primates [14,15] and sciurid rodents [25], and in most cases do not fulfil the guidelines for applying the assumption of trabecular bone as a continuous material ([41]; electronic supplementary material, table S3), they nonetheless represent the largest possible standard sample of trabecular bone available in the vertebrae of our species of interest. Shrews are among the smallest mammals on Earth, [31] and the relatively small space within a shrew vertebral body limits the degree to which trabeculae can interact with one another rather than the cortical shell of the vertebra. This results in a structure that likely behaves less like a cortical shell filled with a cellular solid (e.g. larger mammalian bones; [42,43]), and more like a cortical shell supported by a series of internal struts (e.g. bird forelimb bones [44]). However, the metrics we collected on trabeculae and relative bone density remain relevant to understanding how shrew bones withstand force, including down to the level of individual trabeculae [45], whose shape and capability to resist bending can also be related to BVF [42].

(d) Full-column analysis

All analyses were performed in R v. 3.6.1 [46]. Trends in trabecular bone metrics were compared using goodness-of-fit for polynomial lines, estimated using the stats function lm() and polynomial degrees 1–9. For each metric (e.g. BVF), a polynomial line was fitted to the species mean for that metric through the thoracolumbar column (see electronic supplementary material, figure S10). The purpose of this line fitting was to determine the similarity in the overall pattern of change through the column among the three species. Model fit was assessed with the Akaike information criterion (AIC) and Bayesian information criterion (BIC) from the R package stats, and corrected AIC (AICc) from the package sme [47]. Because we had so few specimens of *S. thori* ($N = 3$, which nonetheless represents the entire known sample of museum specimens worldwide), we used a custom function to subsample sets of 3 *S. somereni* specimens (without replacement) from our total of 8, and calculate the resulting goodness-of-fit for polynomials from degree 1 to 9. We replicated this sampling 100 times to determine if the originally chosen best-fit polynomial and the differences in polynomial fits among species were robust to a small sample size.

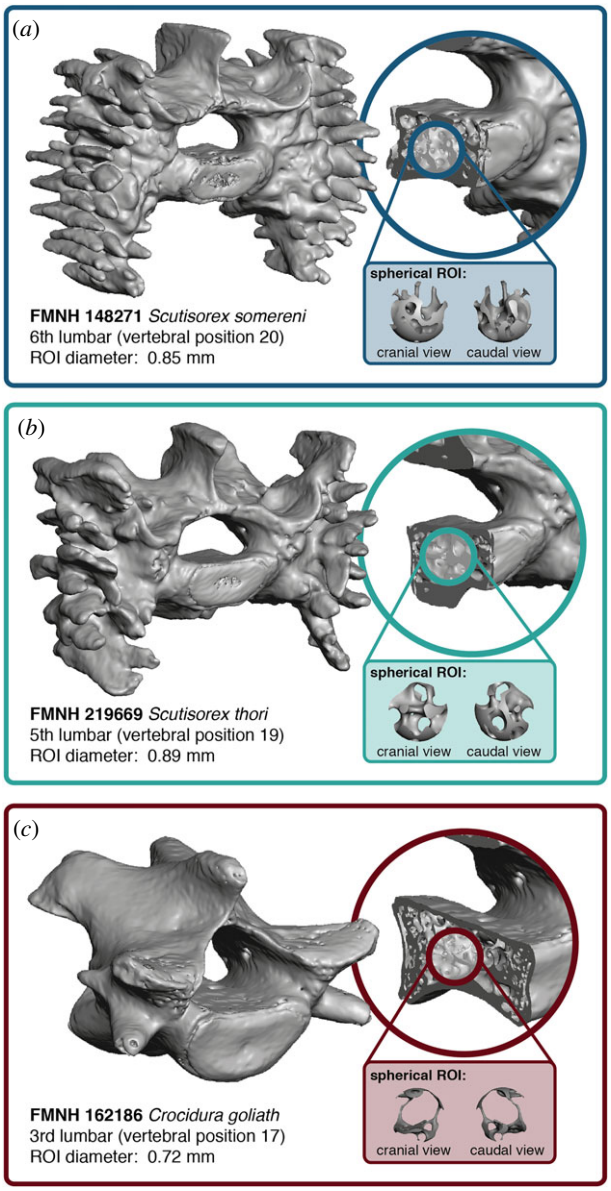

Figure 2. Representative whole bone and region of interest from a mid-column lumbar vertebra of each included species. Vertebrae and ROIs are not to scale. Insets show sagittal sections of each vertebra. (Online version in colour.)

3. Results

(a) External morphology

The total number of dorsal vertebrae ranges from 23 to 25 in *S. somereni*, holds at 22 for all specimens of *S. thori*, and

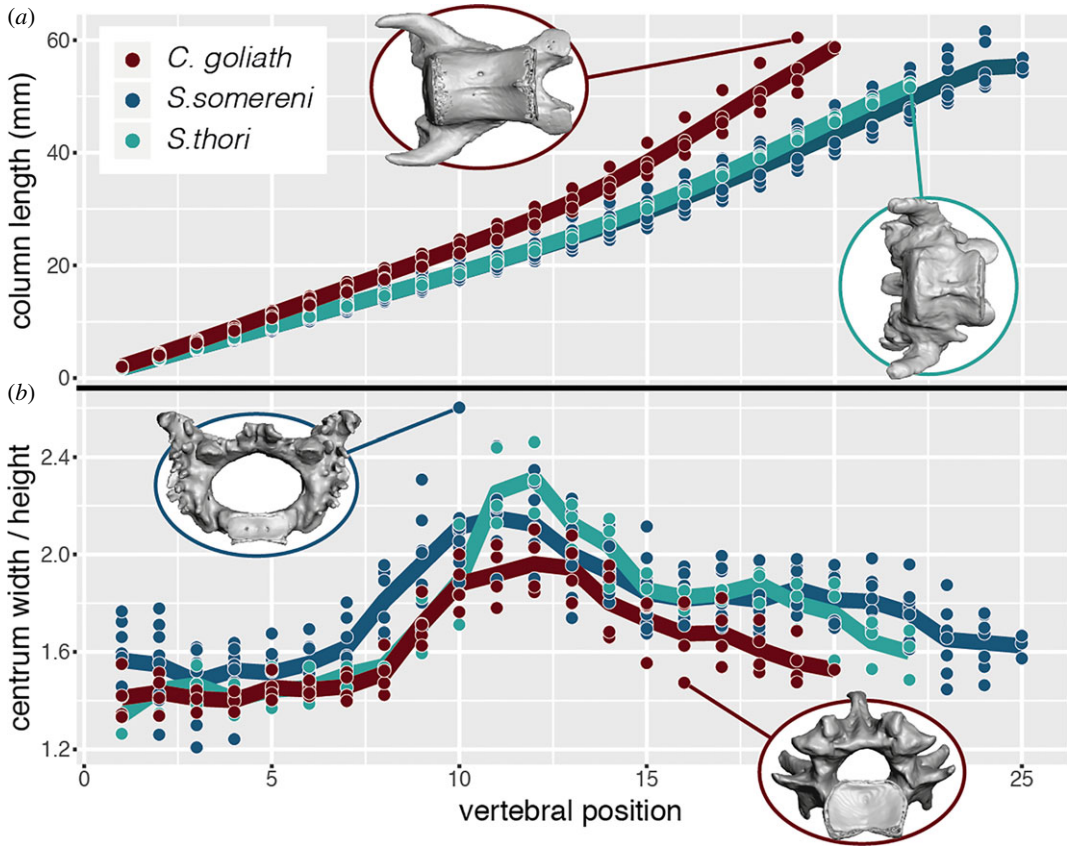

Figure 3. Vertebral centrum dimensions for all specimens. Vertebral position (*x*-axis) starts at position 1 = T01 for each specimen, and continues numerically through all subsequent vertebral positions. The first lumbar position (L01) is at vertebral position 14, 15, or 16, depending on the specimen. Thick lines connect average values for all specimens of a species at a given vertebral position; circles are individual specimens. (*a*) Cumulative centrum length as a proxy vertebral column length, plotted as a function of vertebral position. Specimens are shown in ventral view with cranial to the left: FMNH 162144, *C. goliath* L05; FMNH 222613, *S. thori* L08. (*b*) Ratio of centrum width to height as a function of vertebral position. Specimens are shown in caudal view: FMNH 137613, *S. somereni* T10; FMNH 162144 *C. goliath* L2. (Online version in colour.)

ranges from 19 to 20 in *C. goliath* (table 1). Although *C. goliath* has fewer vertebrae than either species of *Scutisorex*, it has a similar total column length (using cumulative centrum length as a proxy for total length) because of its relatively longer caudal thoracic and lumbar vertebrae (figure 3*a*). Centrum width and height show considerable overlap among the three species in the cranial thoracic column, but all show peak thoracic width at slightly different vertebral positions. Caudal thoracic and lumbar centra in *C. goliath* also tend to be dorsoventrally taller than those of either *Scutisorex* species, with the exception of the caudalmost positions in the latter (L6–12; figure 3*b*). This mirrors qualitative observations of the dorsoventrally compressed, oval cross-section of *Scutisorex* centra.

Overall tubercle counts are higher on average in *S. somereni* than *S. thori* (figure 4). Total tubercle count follows a similar trajectory in both species, increasing from vertebral position 1 to position 15–17 (usually corresponding to a position between L1 and L3) and then decreasing caudally at a similar or slightly faster rate (figure 4*a*). Tubercles are more abundant on the caudal faces of the vertebrae than the cranial faces, but show similar patterns of increase and decrease through the column, largely mirroring the pattern of increase and decrease in total tubercle count (figure 4*a*; electronic supplementary material, figure S9). By contrast, dorsal and ventral tubercle counts show markedly different trajectories of change through the thoracic and lumbar spine (figure 4*b*). Dorsal tubercles appear around vertebral position 3–5 and peak at position 11 (T11). Ventral tubercles do not appear until position 9–10, and peak higher than the maximum for dorsal tubercles, around position 15–17 (approx. L1–L3). The number of tubercles on both the dorsal and ventral sides of the vertebrae drops off precipitously in the last few lumbar positions. This region functions as the hinge between the lumbar spine and pelvis and serves as an attachment point for increased musculature surrounding the lumbosacral joint and hind limbs (e.g. psoas major lateralis and psoas minor, [1]; figs 3 and 5). Despite the increased flexibility in this region, especially at the lumbosacral joint, there are still sufficient tubercles present on the caudalmost lumbar vertebrae to stop nearly all axial torsion at intervertebral joints.

(b) Internal morphology: trabecular bone architecture, interspecific differences, and polynomial model fitting

TBA metrics vary differently across the dorsal vertebral column, and their patterns also differ among species. BVF in both *Scutisorex* species decreases in the first five vertebral positions before undergoing a slight increase and then remaining relatively constant from position 10 onward (figure 5*a*). Although BVF follows similar trajectories in both species, and the two have some overlapping values, as well as overlapping areas of uncertainty, overall BVF is higher in *S. somereni* than in *S. thori*. In *C. goliath*, BVF generally decreases through the whole column, and BVF values in *C. goliath* are lower

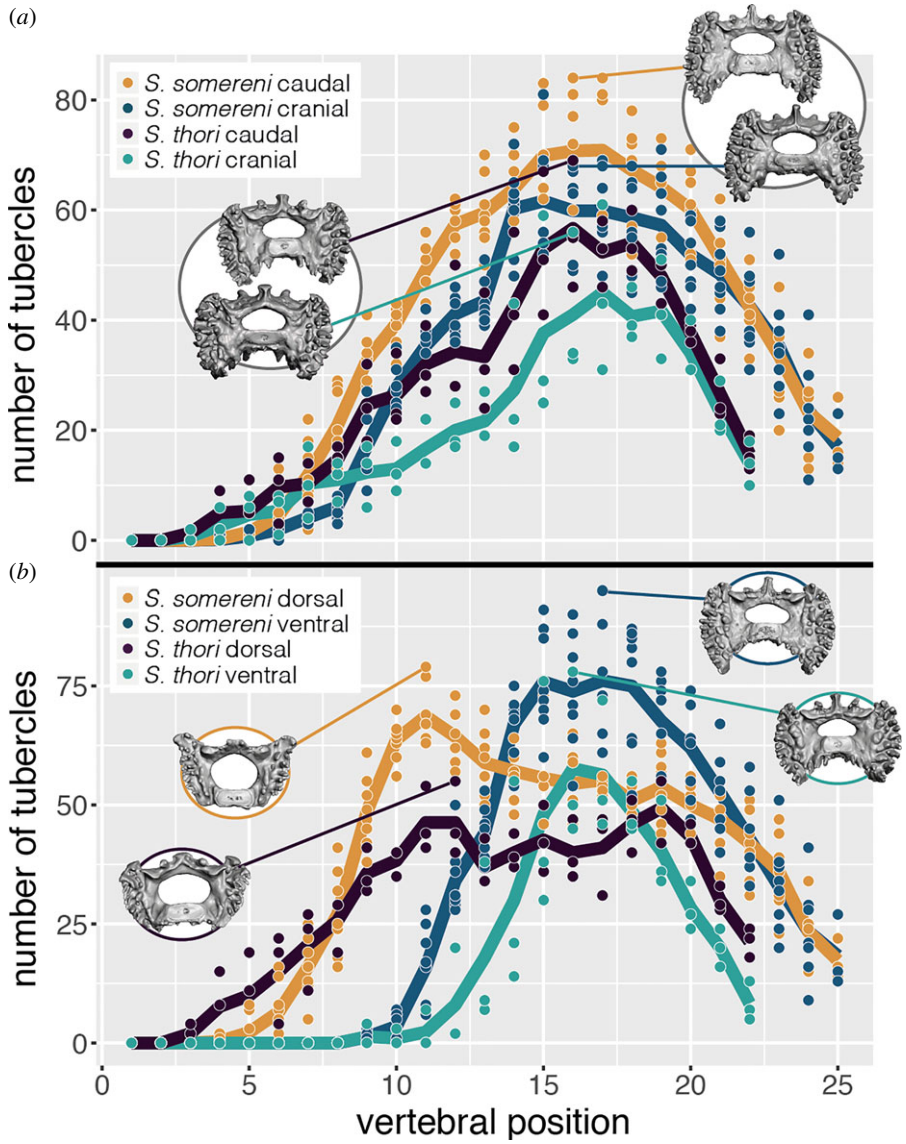

Figure 4. Number of tubercles on *Scutisorex* vertebrae by species and vertebral position. Vertebral position (*x*-axis) is the same as figure 3. Thick lines connect average values for all specimens of a species at a given vertebral position; circles are individual specimens. (*a*) Number of tubercles on cranial versus caudal faces of the vertebrae. Specimens shown are the same vertebra in both cranial (bottom) and caudal (top) view: FMNH 222612, *S. thori* L01; FMNH 148271, *S. somereni* L02. (*b*) Number of tubercles on dorsal versus ventral sections of the vertebrae. Specimens are shown in caudal view and are as follows, clockwise from lower left: FMNH 222612 *S. thori* T12, FMNH 148941 *S. somereni* T11, 148941 L03, 222612 L02. (Online version in colour.)

than those of either species of *Scutisorex*, such that there is almost no range overlap between *C. goliath* and *S. thori* from position 7 onward, and nearly no overlap in uncertainty around the species means. Tb.N generally decreases through the column in *C. goliath* and *S. thori*, whereas in *S. somereni*, Tb.N increases from position 4 to 14, followed by a decrease to the end of the column (figure 5*b*). In terms of absolute value, means for *C. goliath* and *S. thori* are quite similar to one another through the whole column, but *S. somereni* has consistently higher mean Tb.N values from position 9 onward, with a local maximum at position 14, just one position cranial to the peak in tubercle number in that species (figure 4*a*). Tb.Th is higher in *Scutisorex* than in *C. goliath* (figure 5*c*), especially in the more caudal thoracic and lumbar vertebrae. The mean Tb.Th also mostly decreases through the vertebral column in *C. goliath*, whereas it increases in *S. thori* and *S. somereni*.

Polynomial line fits were chosen using BIC because it made the most consistent choices for the subsampled *S. somereni* data (electronic supplementary material, table S4). Because BIC exacts a stronger penalty than AIC for additional model parameters, it consistently chose the same or lower-degree polynomial models (table 2; electronic supplementary material, table S5), and is therefore a more conservative choice than AIC or AICc with our small sample size. According to BIC, *C. goliath* and *S. thori* exhibit more similar patterns in BVF through the dorsal vertebral column, whereas for Tb.N, all three species have slightly different patterns: second degree for *S. thori*, first degree for *C. goliath*, and fourth degree for *S. somereni*. *Crocidura goliath* and *S. somereni* follow a linear trajectory for Tb.Th, whereas *S. thori* has a more complex pattern (figure 5; electronic supplementary material, figure S10). Chosen polynomial models for *S. somereni* are robust to subsampling combinations of three specimens (electronic supplementary material, table S4), indicating that differences among the three species are unlikely to stem from insufficient sampling.

Primary trabecular direction is largely aligned with the craniocaudal axis of the vertebral centrum in both thoracic and lumbar vertebrae of *S. somereni* and *S. thori*, and, to a lesser degree, the thoracic vertebrae of *C. goliath* (figure 6). Trabecular orientation in the lumbar vertebrae of *C. goliath*

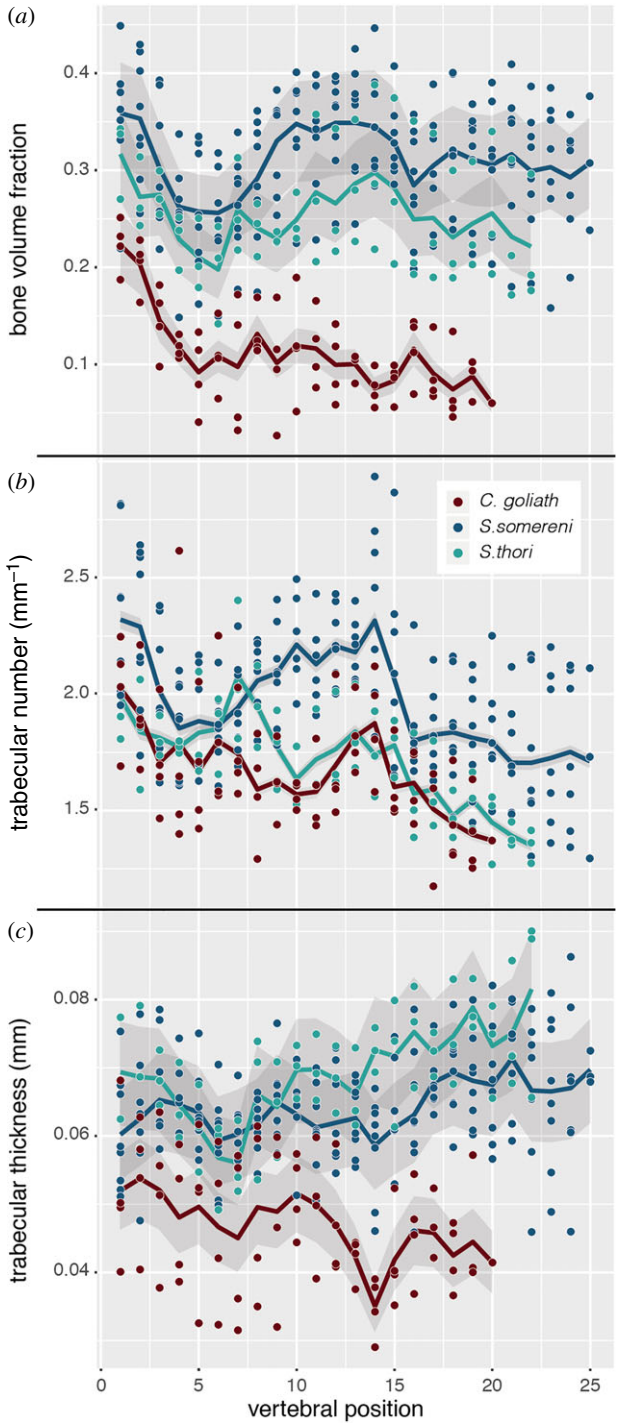

Figure 5. Trabecular bone metrics for all vertebrae and species. Vertebral position (*x*-axis) is the same as figures 3 and 4. Thick lines connect average values for all specimens of a species at a given vertebral position; circles are individual specimens. Shaded regions behind averages are ranges of uncertainty (see text for details on uncertainty calculations). (Online version in colour.)

is much more irregular, and has no strong association with anatomical directions (figure 6).

4. Discussion

(a) Evidence of elevated axial compressive load in *Scutisorex*

The TBA of the centra of both *Scutisorex* species indicates that they are subjected to greater axial compressive loads than

Table 2. AIC, AICc, and BIC degree of best-fit polynomial models of change in trabecular bone metrics through the thoracic and lumbar spine in *S. somereni*, *S. thori*, and *C. goliath*. Numbers in bold show where two species have the same degree of chosen best-fit model for a given variable.

		polynomial model degree		
TBA metric	taxon	AIC	AICc	BIC
bone volume fraction	*Scutisorex somereni*	**7**	7	7
	Scutisorex thori	4	**4**	**4**
	Crocidura goliath	**7**	**4**	**4**
trabecular number	*Scutisorex somereni*	7	7	4
	Scutisorex thori	2	2	2
	Crocidura goliath	3	3	1
trabecular thickness	*Scutisorex somereni*	**4**	4	**1**
	Scutisorex thori	**4**	3	3
	Crocidura goliath	1	1	**1**

the vertebrae of *C. goliath*. However, as with its external morphology ([2]; this study), *S. thori* is intermediate in trabecular morphology between *S. somereni* and *C. goliath* in several respects. Both *Scutisorex* species have higher BVF than *C. goliath* through almost the entire dorsal vertebral series, but the mean values for *S. thori* are between those of *S. somereni* and *C. goliath*, and overall trends in BVF through the column are more similar between *S. thori* and *C. goliath* (figure 5*a* and table 2). BVF is an effective predictor of Young's modulus and strength in human trabecular bone, with higher BVF generally corresponding to stronger and stiffer bone [48–50]. Nevertheless, BVF does not fully describe the structure of trabecular bone, and is a better predictor of mechanical properties when considered with other microstructural characteristics [48]. Besides having higher BVF than *C. goliath*, both *Scutisorex* species have higher Tb.Th (but with slightly different trends through the column; table 2). Higher Tb.Th also correlates to higher compressive strength in the lumbar spine of humans [51]. Further, increased cyclical bone loading has been shown to result in increased BVF and Tb.Th in mouse vertebrae [52], an indication that the higher values in *Scutisorex* likely relate to more frequent, higher-magnitude loads. In contrast with the gradient in BVF (lowest in *C. goliath*, moderate in *S. thori*, highest in *S. somereni*), the pattern in Tb.Th is much more similar in the two species of *Scutisorex*, with *C. goliath* alone having a much lower average through the column (figure 5*c*). This is an even more intriguing pattern in light of pattern of change in Tb.N (figure 5*b* and table 2). *Scutisorex thori* and *C. goliath* change through the dorsal column with almost identical values and patterns, whereas *S. somereni* has higher Tb.N than both *S. thori* and *C. goliath*, especially in the caudal thoracic and cranial lumbar positions. This pattern is of special interest because a given value for BVF can be achieved with several different configurations of trabecular structure (e.g. fewer but thicker trabeculae versus more numerous but thinner trabeculae). Two- and three-dimensional finite-element models have shown that a change in BVF accomplished primarily by altering Tb.N has a greater effect on Young's modulus and bone strength than the same

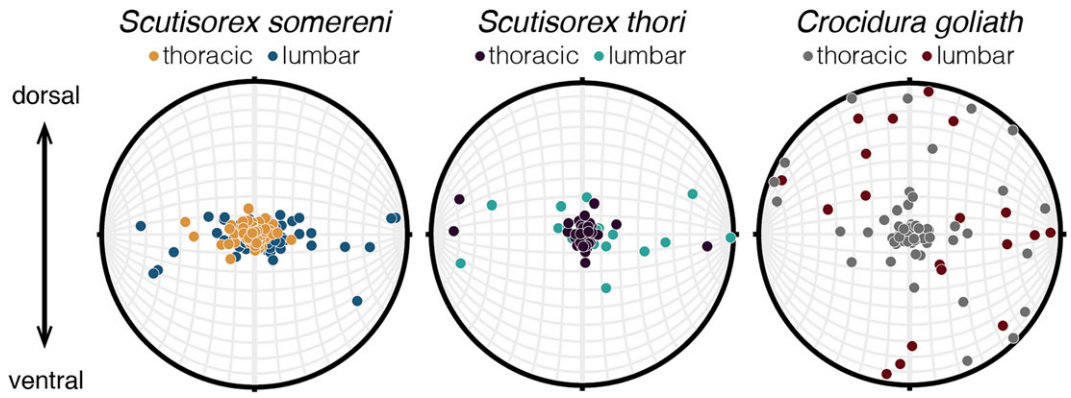

Figure 6. Hemispherical plots of primary trabecular orientation for each vertebral ROI. Points closer to the centre of the plot represent a vertebra with trabecular orientation closer to parallel with the craniocaudal axis of the centrum. (Online version in colour.)

change in BVF accomplished via alteration of Tb.Th [53–55]. As such, despite its intermediate BVF, *S. thori* could have trabecular bone mechanical properties slightly closer to those of *C. goliath* because its Tb.N is closer to that of *C. goliath*. Likewise, because change in Tb.N has a greater effect on the mechanical properties of trabecular bone than change in Tb.Th [54,55], if *S. thori* exhibited the same BVF, but a Tb.N closer to that of *S. somereni* and Tb.Th more similar to that of *C. goliath*, we might expect its trabecular bone to have mechanical properties more similar to *S. somereni*.

Based on the findings outlined above, we expect that the vertebral trabecular bone of *S. somereni* and *S. thori* are both stronger and stiffer under *in vivo* forces than that of *C. goliath*. However, the anisotropic qualities of bone must be accounted for when considering loading schemes. Anisotropic materials behave differently when forces are applied from different directions. In the vertebrae of a quadruped mammal, the primary load is craniocaudal compression, which allows the animal to maintain its posture [56]. To withstand deformation under this load, we might expect the primary direction of trabecular elements in the vertebral centrum to be along the craniocaudal axis [57]. We found that the primary trabecular orientation in *Scutisorex* is much more closely aligned with the craniocaudal axis of the vertebral centrum than in *C. goliath* (figure 6). This could be due in part to the low BVF values and small ROI size in *C. goliath*: some ROIs capture only a single trabecular element, making assessment of the continuous trabecular structure difficult [41]. However, if low BVF is the reason for the difference in measured orientation, we might expect that *S. thori*, which has an intermediate BVF, to have an intermediate tendency for craniocaudal trabecular orientation. This does not appear to be the case (figure 6). It is possible that the interlocking tubercles on the vertebrae of *Scutisorex* spp. also play a role in the signal detected here, restricting the primary trabecular direction through restriction of the overall intervertebral range of motion. Further *in vitro* or *in silico* tests will be required to determine the degree to which range of motion of an intervertebral joint, and craniocaudal alignment of trabeculae in its component vertebrae, are correlated.

(b) Whole-bone morphology and adaptations for stereotyped spinal flexion

Scutisorex somereni has a number of specialized muscles for fine control of axial compression in the spine, including the m. intertubercularis ([1], fig. 2), which connects tubercles on adjacent vertebrae, and the m. tuberculoventralis, which connects the ventral tubercles of a vertebra to the ventral side of the centrum on a more cranial vertebra [1]. Additionally, under compression, *S. somereni* intervertebral joints lose their viscoelastic qualities and begin to behave mechanically as an immobile, solid unit [8]. If the joint bends, it does so almost exclusively in dorsoventral flexion. This restriction of intervertebral motion to flexion in the sagittal plane relies on robust hypaxial musculature [1] and a suite of whole-bone characteristics that resist bending, torsion, and extension.

In the craniocaudal view, the vertebrae with the largest number of tubercles (caudal thoracic through cranial lumbar positions) resemble an I-beam in cross-section (figure 2). This structure has a large second moment of area that is exceptionally capable of resisting bending perpendicular to its flange, here formed by the dorsoventral expansion of the transverse process. This expansion of the transverse process is relatively larger in *S. somereni* than *S. thori*, resulting in not only more points of contact between adjacent vertebrae (more tubercles; figure 4) to interlock and resist axial torsion, but also a beam cross-section with a greater concentration of material away from the neutral axis, and potentially better resistance to deformation under mediolateral bending.

The increased number of dorsal tubercles in the caudalmost thoracic vertebrae of both species, along with an additional v-shaped joint between the neural spines of adjacent vertebrae in the caudal thoracics [4,5] hint at a greater need to resist extension in this region using only the dorsal side of the column. This region also shows a local peak in Tb.N in both *Scutisorex* species (figure 5), suggesting additional centrum strength in compression. The automatic interdigitation of dorsal tubercles would be useful for resisting both extension and shear if the animal were undergoing an external, ventrally directed load positioned at the top of the kyphosis (like the load proposed in [2]), but it is unclear how that load would be transmitted through the limb girdles and the limbs themselves, which do not appear to be specialized to resist extreme forces [7].

Although we cannot yet identify a specific behaviour associated with the spinal morphology of *Scutisorex*, our results suggest that spinal flexion, and the vertebral compression associated with flexion, are important parts of the animal's lifestyle and/or locomotion. *Scutisorex somereni* has been variously described as having a 'decidedly unsoricid' body motion [1], and a ''trotting' (rather than 'crawling')

gait under an extraordinarily hunched posture' [58]. Passive bending of the spine also suggests a much greater range of motion in sagittal flexion than in sagittal extension or lateral bending [1]. How these qualitative descriptions translate into vertebral kinematics, and how spinal structure plays into the animal's unique locomotion, are yet to be fully investigated. The posture, gait, and spinal musculature of *S. thori* are poorly known compared to those of *S. somereni*, and may provide additional support for the hypothesis that the *S. thori* spine is functionally intermediate.

5. Conclusion

Determining the function of extreme morphologies is a quintessential challenge in organismal biology. We have shown here that the plastic mechanical properties of trabecular bone provide insight into the *in vivo* use of unusually modified bones, despite a lack of clear external homologies in functional structures. Our synthesis of data on the internal and external structure of *Scutisorex* vertebrae with the existing literature reveals that: (i) *Scutisorex* vertebrae likely undergo axial compressive forces that are higher in frequency and/or magnitude than the forces acting on *C. goliath* vertebrae, (ii) besides being intermediate in external morphology, *S. thori* is probably also functionally intermediate between *S. somereni* and *C. goliath*, based on TBA and external tubercle morphology, and (iii) there is correspondence between peaks in *Scutisorex* tubercle number and TBA, particularly Tb.N. Because our understanding of the respective functions of trabecular bone and cortical bone in very small mammals is limited, and behavioural information on *Scutisorex* is scant, much remains to be discovered about this enigmatic genus of shrews. Our work provides a starting point for additional tests of how *Scutisorex* and other small mammals experience force, as well as a new approach for tracking the evolution of function in morphologically extreme vertebrates.

Data accessibility. Trabecular bone architecture data and external vertebral measurements, including tubercle counts, as well as raw data from segmentation sensitivity and uncertainty tests, are available on the Dryad Digital Repository: https://doi.org/10.5061/dryad.8w9ghx3hf [59]. A µCT scan regions of interest (ROIs), and 3D STL models of *Scutisorex* vertebrae used in this study, are available for download at the online repository Morphosource (https://www.morphosource.org/Detail/ProjectDetail/Show/project_id/956).

Competing interests. We declare we have no competing interests.

Authors' contributions. S.M.S. and K.D.A. conceived the study; S.M.S. designed the study, selected specimens, performed µCT scans, and carried out segmentation and data analysis; K.D.A. consulted on data collection and analysis; S.M.S. and K.D.A. wrote the manuscript.

Funding. S.M.S. was supported by a National Science Foundation Postdoctoral Fellowship in Biology (grant no. DBI-1811627).

Acknowledgements. We thank S. Briones, J. Esselstyn, A. Ferguson, L. Heaney, K. Jones, J. Kerbis Peterhans, Z.-X. Luo, A. Neander, B. Patterson, J. Phelps, L. Smith, S. Swartz, K. Stanchak, and E. Zack for helpful discussions regarding this work; access to µCT facilities and scanning assistance; access to FMNH specimens and field notes; and assistance with German translation. We also thank all current and past collectors who have contributed specimens to the FMNH mammalogy collections, without whom this work would not be possible; and two anonymous reviewers, whose comments and suggestions greatly improved this manuscript.

References

1. Cullinane DM, Aleper D. 1998 The functional and biomechanical modifications of the spine of *Scutisorex somereni*, the hero shrew: spinal musculature. *J. Zool.* **244**, 453–458. (doi:10.1017/S0952836998003161)
2. Stanley WT *et al.* 2013 A new hero emerges: another exceptional mammalian spine and its potential adaptive significance. *Biol. Lett.* **9**, 20130386. (doi:10.1098/rsbl.2013.0486)
3. Thomas O. 1910 XII.—A new genus of fruit-bats and two new shrews from Africa. *Ann. Mag. Nat. Hist.* **6**, 111–114. (doi:10.1080/00222931008692827)
4. Allen JA, Lang H, Chapin JP. 1917 The skeletal characters of *Scutisorex* Thomas. *Bull. AMNH* **37**, article 28.
5. Schulte H von W, Lang H, Chapin JP. 1917 A note on the lumbar vertebrae of *Scutisorex* Thomas. *Bull. AMNH* **37**, article 29.
6. Ahmed A, Klima M. 1978 The development and function of the lumbar vertebrae of the hero shrew *Scutisorex somereni* (Thomas 1910). *Zeitschrift Saugetierkd.* **43**, 1–17.
7. Cullinane DM, Aleper D, Bertram JEA. 1998 The functional and biomechanical modifications of the spine of *Scutisorex somereni*, the hero shrew: skeletal scaling relationships. *J. Zool.* **244**, 447–452. (doi:10.1111/j.1469-7998.1998.tb00049.x)
8. Cullinane DM, Bertram JEA. 2000 The mechanical behavior of a novel mammalian intervertebral joint. *J. Anat.* **197**, 627–634. (doi:10.1017/S0021878299006986)
9. Churchfield S, Dieterlen F, Hutterer R, Dudu A. 2007 Feeding ecology of the armored shrew, from the north-eastern Democratic Republic of Congo. *J. Zool.* **273**, 40–45. (doi:10.1111/j.1469-7998.2007.00297.x)
10. Wolff J. 1893 Das gesetz der transformation der knochen. *DMW-Deutsche Medizinische Wochenschrift* **19**, 1222–1224. (doi:10.1055/s-0028-1144106)
11. Cowin SC. 1986 Wolff's law of trabecular architecture at remodeling equilibrium. *J. Biomech. Eng.* **108**, 83–88. (doi:10.1115/1.3138584)
12. Huiskes R, Rulmerman R, Van Lenthe GH, Janssen JD. 2000 Effects of mechanical forces on maintenance and adaptation of form in trabecular bone. *Nature* **405**, 704–706. (doi:10.1038/35015116)
13. Ruff C, Holt B, Trinkaus E. 2006 Who's afraid of the big bad Wolff?: 'Wolff's law' and bone functional adaptation. *Am. J. Phys. Anthropol. Off. Publ. Am. Assoc. Phys. Anthropol.* **129**, 484–498. (doi:10.1002/ajpa.20371)
14. Zysset PK, Goulet RW, Hollister SJ. 1998 A global relationship between trabecular bone morphology and homogenized elastic properties. *J. Biomech. Eng.* **120**, 640–646. (doi:10.1115/1.2834756)
15. Cotter MM, Simpson SW, Latimer BM, Hernandez CJ. 2009 Trabecular microarchitecture of hominoid thoracic vertebrae. *Anat. Rec.* **292**, 1098–1106. (doi:10.1002/ar.20932)
16. Ryan TM, Shaw CN. 2012 Unique suites of trabecular bone features characterize locomotor behavior in human and non-human anthropoid primates. *PLoS ONE* **7**, e41037. (doi:10.1371/journal.pone.0041037)
17. Ryan TM, Shaw CN. 2015 Gracility of the modern *Homo sapiens* skeleton is the result of decreased biomechanical loading. *Proc. Natl Acad. Sci. USA* **112**, 372–377. (doi:10.1073/pnas.1418646112)
18. Saers JPP, Cazorla-Bak Y, Shaw CN, Stock JT, Ryan TM. 2016 Trabecular bone structural variation throughout the human lower limb. *J. Hum. Evol.* **97**, 97–108. (doi:10.1016/j.jhevol.2016.05.012)
19. Gauthier R, Langer M, Follet H, Olivier C, Gouttenoire PJ, Helfen L, Rongiéras F, Mitton D, Peyrin F. 2018 3D micro structural analysis of human cortical bone in paired femoral diaphysis, femoral neck and radial diaphysis. *J. Struct. Biol.* **204**, 182–190. (doi:10.1016/j.jsb.2018.08.006)

20. Tanck E, Homminga J, Van Lenthe GH, Huiskes R. 2001 Increase in bone volume fraction precedes architectural adaptation in growing bone. *Bone* **28**, 650–654. (doi:10.1016/S8756-3282(01)00464-1)
21. Mittra E, Rubin C, Qin YX. 2005 Interrelationship of trabecular mechanical and microstructural properties in sheep trabecular bone. *J. Biomech.* **38**, 1229–1237. (doi:10.1016/j.jbiomech.2004.06.007)
22. Barak MM, Lieberman DE, Hublin JJ. 2011 A Wolff in sheep's clothing: trabecular bone adaptation in response to changes in joint loading orientation. *Bone* **49**, 1141–1151. (doi:10.1016/j.bone.2011.08.020)
23. Van Der Meulen MCH, Morgan TG, Yang X, Baldini TH, Myers ER, Wright TM, Bostrom MPG. 2006 Cancellous bone adaptation to *in vivo* loading in a rabbit model. *Bone* **38**, 871–877. (doi:10.1016/j.bone.2005.11.026)
24. Van Der Meulen MCH, Yang X, Morgan TG, Bostrom MPG. 2009 The effects of loading on cancellous bone in the rabbit. *Clin. Orthop. Relat. Res.* **467**, 2000–2006. (doi:10.1007/s11999-009-0897-4)
25. Mielke M, Wölfer J, Arnold P, Van Heteren AH, Amson E, Nyakatura JA. 2018 Trabecular architecture in the sciuromorph femoral head: allometry and functional adaptation. *Zool. Lett.* **4**, 1–11. (doi:10.1186/s40851-018-0093-z)
26. Mielke M, Nyakatura JA. 2019 Bone microstructure in finite element modeling: the functional role of trabeculae in the femoral head of *Sciurus vulgaris*. *Zoomorphology* **138**, 535–547. (doi:10.1007/s00435-019-00456-2)
27. Swartz SM, Parker A, Huo C. 1998 Theoretical and empirical scaling patterns and topological homology in bone trabeculae. *J. Exp. Biol.* **201**, 573–590.
28. Iwamoto J, Yeh JK, Aloia JF. 1999 Differential effect of treadmill exercise on three cancellous bone sites in the young growing rat. *Bone* **24**, 163–169. (doi:10.1016/S8756-3282(98)00189-6)
29. Sugiyama T, Price JS, Lanyon LE. 2010 Functional adaptation to mechanical loading in both cortical and cancellous bone is controlled locally and is confined to the loaded bones. *Bone* **46**, 314–321. (doi:10.1016/j.bone.2009.08.054)
30. Barak MM, Weiner S, Shahar R. 2010 The contribution of trabecular bone to the stiffness and strength of rat lumbar vertebrae. *Spine (Phila. Pa. 1976)* **35**, 1153–1159. (doi:10.1097/BRS.0b013e3181e5e34b)
31. Barak MM, Lieberman DE, Hublin JJ. 2013 Of mice, rats and men: trabecular bone architecture in mammals scales to body mass with negative allometry. *J. Struct. Biol.* **183**, 123–131. (doi:10.1016/j.jsb.2013.04.009)
32. Doube M, Kłosowski MM, Wiktorowicz-Conroy AM, Hutchinson JR, Shefelbine SJ. 2011 Trabecular bone scales allometrically in mammals and birds. *Proc. R. Soc. B* **278**, 3067–3073. (doi:10.1098/rspb.2011.0069)
33. Schindelin J *et al.* 2012 Fiji: an open-source platform for biological-image analysis. *Nat. Methods* **9**, 676–682. (doi:10.1038/nmeth.2019)
34. Otsu N. 1979 Threshold selection method from gray-level histograms. *IEEE Trans. Syst. Man. Cybern. SMC* **9**, 62–66. (doi:10.1109/tsmc.1979.4310076)
35. Kivell TL, Skinner MM, Lazenby R, Hublin JJ. 2011 Methodological considerations for analyzing trabecular architecture: an example from the primate hand. *J. Anat.* **218**, 209–225. (doi:10.1111/j.1469-7580.2010.01314.x)
36. Hara T, Tanck E, Homminga J, Huiskes R. 2002 The influence of microcomputed tomography threshold variations on the assessment of structural and mechanical trabecular bone properties. *Bone* **31**, 107–109. (doi:10.1016/S8756-3282(02)00782-2)
37. Ketcham RA, Ryan TM. 2004 Quantification and visualization of anisotropy in trabecular bone. *J. Microsc.* **213**, 158–171. (doi:10.1111/j.1365-2818.2004.01277.x)
38. Ketcham RA. 2005 Three-dimensional grain fabric measurements using high-resolution X-ray computed tomography. *J. Struct. Geol.* **27**, 1217–1228. (doi:10.1016/j.jsg.2005.02.006)
39. Allmendinger RW, Cardozo N, Fisher DM. 2011 *Structural geology algorithms: vectors and tensors*. Cambridge, UK: Cambridge University Press.
40. Cardozo N, Allmendinger RW. 2013 Spherical projections with OSXStereonet. *Comput. Geosci.* **51**, 193–205. (doi:10.1016/j.cageo.2012.07.021)
41. Harrigan TP, Jasty M, Mann RW, Harris WH. 1988 Limitations of the continuum assumption in cancellous bone. *J. Biomech.* **21**, 269–275. (doi:10.1016/0021-9290(88)90257-6)
42. Gibson LJ. 1985 The mechanical behaviour of cancellous bone. *J. Biomech.* **18**, 317–328. (doi:10.1016/0021-9290(85)90287-8)
43. Gibson LJ. 2005 Biomechanics of cellular solids. *J. Biomech.* **38**, 377–399. (doi:10.1016/j.jbiomech.2004.09.027)
44. Novitskaya E, Ruestes CJ, Porter MM, Lubarda VA, Meyers MA, McKittrick J. 2017 Reinforcements in avian wing bones: experiments, analysis, and modeling. *J. Mech. Behav. Biomed. Mater.* **76**, 85–96. (doi:10.1016/j.jmbbm.2017.07.020)
45. Townsend PR, Rose RM, Radin EL. 1975 Buckling studies of single human trabeculae. *J. Biomech.* **8**, 199–201. (doi:10.1016/0021-9290(75)90025-1)
46. R Core Team. 2019 *R: a language and environment for statistical computing*. Vienna, Austria: R Foundation for Statistical Computing.
47. Berk M. 2018 sme: smoothing-splines mixed-effects models. R package version 1.0.2.
48. Ulrich D, Van Rietbergen B, Laib A, Ruegsegger P. 1999 The ability of three-dimensional structural indices to reflect mechanical aspects of trabecular bone. *Bone* **25**, 55–60. (doi:10.1016/S8756-3282(99)00098-8)
49. Keller TS, Carter DR, Hernandez CJ, Beaupre GS. 2001 The influence of bone volume fraction and ash fraction on bone strength and modulus. *Bone* **29**, 74–78. (doi:10.1016/S8756-3282(01) 00467-7)
50. Nazarian A, Von Stechow D, Zurakowski D, Müller R, Snyder BD. 2008 Bone volume fraction explains the variation in strength and stiffness of cancellous bone affected by metastatic cancer and osteoporosis. *Calcif. Tissue Int.* **83**, 368–379. (doi:10.1007/s00223-008-9174-x)
51. Vesterby A, Mosekilde L, Gundersen HJG, Melsen F, Mosekilde L, Holme K, Sørensen S. 1991 Biologically meaningful determinants of the *in vitro* strength of lumbar vertebrae. *Bone* **12**, 219–224. (doi:10.1016/8756-3282(91)90044-J)
52. Lambers FM, Schulte FA, Kuhn G, Webster DJ, Müller R. 2011 Mouse tail vertebrae adapt to cyclic mechanical loading by increasing bone formation rate and decreasing bone resorption rate as shown by time-lapsed *in vivo* imaging of dynamic bone morphometry. *Bone* **49**, 1340–1350. (doi:10.1016/j.bone.2011.08.035)
53. Silva MJ, Gibson LJ. 1997 Modeling the mechanical behavior of vertebral trabecular bone: effects of age-related changes in microstructure. *Bone* **21**, 191–199. (doi:10.1016/S8756-3282(97)00100-2)
54. Vajjala S, Kraynik AM, Gibson LJ. 2000 A cellular solid model for modulus reduction due to resorption of trabeculae in bone. *J. Biomech. Eng.* **122**, 511–515. (doi:10.1115/1.1289996)
55. Guo XE, Kim CH. 2002 Mechanical consequence of trabecular bone loss and its treatment: a three-dimensional model simulation. *Bone* **30**, 404–411. (doi:10.1016/S8756-3282(01)00673-1)
56. Smit TH. 2002 The use of a quadruped as an *in vivo* model for the study of the spine—biomechanical considerations. *Eur. Spine J.* **11**, 137–144. (doi:10.1007/s005860100346)
57. Smit TH, Odgaard A, Schneider E. 1997 Structure and function of vertebral trabecular bone. *Spine (Phila. Pa. 1976)* **22**, 2823–2833. (doi:10.1097/00007632-199712150-00005)
58. Kingdon J. 2015 *The Kingdon field guide to African mammals*. London, UK: Bloomsbury Publishing.
59. Smith SM, Angielczyk KD. 2020 Data from: Deciphering an extreme morphology: bone microarchitecture of the Hero Shrew backbone (Soricidae: *Scutisorex*). Dryad Digital Repository. (doi:10.5061/dryad.8w9ghx3hf)